COMSOL CONFERENCE 2023 MUNICH

Benefit Of Vapor Consideration For LPBF Additive Manufacturing Process Simulation

Morgan Dal[1], Julien Daligault[1], Jérémie Girardot[2]
[1]Laboratoire PIMM, Arts et Metiers Institute of Technology, CNRS, Cnam, HESAM Universite
[2]I2M, Arts et Metiers Institute of Technology, University of Bordeaux, CNRS, Bordeaux INP, INRAE

Abstract
Simulation of laser processes are more and more efficient. In some cases, as welding and additive manufacturing, the physical phenomena are complex, multi-physics and multi-phases, thus some assumptions have to be done. For Laser Powder Bed Fusion, a laser beam melts and vaporizes the substrate and powder materials. In literature, the vaporization process is supposed to produce a recoil pressure at the surface of the liquid, but the momentum created on the gas is usually neglected. In the present paper, authors focus on this part of the model in order to prove the benefit of such consideration. The whole model is described (heat transfers, fluid flows, phase field) and the vapor consideration is detailed physically and numerically for two assumptions: pressure model and momentum model. After having shown some numerical comparisons illustrating the benefit of this method, a short physical analysis is made to conclude on the sensitivity of the vaporization phenomenon on the process.

Keywords: Laser Powder Bed Fusion, Vaporization, Recoil Pressure, Java Programming.

Introduction
The Laser Powder Bed Fusion (LPBF) or Selective Layer Melting (SLM), is one of the laser based additive manufacturing (AM) processes. It is a sequential process with a final workpiece, built layer by layer [1]. A “layer” is the spreading of a few micrometers of metal powder and this last is selectively molten by laser, track after track making a workpiece slice. The particularity and the strength of this process is the weak rugosity of the built compared to other AM process (Laser Metal Deposition or Wire Arc Additive Manufacturing, for instance). Nevertheless, the single-track quality has an effect horizontally on other tracks of the same layer and vertically on the next layer tracks. For instance, the main defects are pore generation due to local lack of powder (denudation) or particles aggregated on the bed (due to spatters) and drift of sample dimension due to flow instabilities or mechanical effects (not treated here) [2 - 4]. All of them can be related to single track quality.

More generally, since 10 – 20 years, additive manufacturing or metallic 3D printing is one of the most growing industrial technologies [5 - 6]). As the industrial machines are now easily available and as the heavy industry (energy, automotive, aircraft, …) is trying to master these processes to ensure pieces quality, a lot of experimental studies are appearing in this research field. Nevertheless, for powder bed technologies, experimental investigations illustrate some difficulties in terms defects visualization and analyze. Indeed, due to the small size of the powder and of the molten pool, due to the powder masking effect and due to the compacity of the building chambers, it still difficult to have a pertinent and efficient experimental setup with diagnostics (high speed imaging, IR camera, …). In this context, numerical approach can give some information and explanations.

As explain in a previous work [7], the process stability or instabilities is highly dependent of the elementary single-track quality and the mesoscale analysis is an interesting point of view. Moreover, as it is largely multiphysics (laser beam, heat transfers, fluid flows, …) and multiphase (bulk, powder, gas) it is also a complex case to be analyzed numerically. Thus, some common but strong assumptions can be found in the literature, concerning the powder behavior ([8-10]), and thermal properties ([11-12]). More recently, some researchers have considered the whole particles of a part of the powder layer in their simulations ([13], [14], [15], [7], [1]). Our previous work on this topic was presented at the Comsol Conference 2020 [7] and the conclusions were, the methodology to import powder is quite realistic, the beam reflection on the material and the vapor jet can probably have an effect on the melt pool shape. In the present work, authors focus on recent developments on the way to produce vapor jet on the model and how it sensitive.

In this paper, authors describe a mesoscale (static spot) model of LPBF able to simulate some process behavior and giving some process answers. As a ray tracing method has already been done in previous works assuming a homogenized powder [16] or in case of welding [17] authors will focus here on the powder particular description and vapor jet modeling. After having justified several assumptions, recalled the methodology used to import particles from DEM (Discrete Element Method) calculation, the physical phenomena will be recalled, and numerical setup will be described. Then, the results in terms of molten zones for two formulation assumptions will be shown and discussed.

Theory
As this work focus on the mesoscale aspects of the process (one track), the physical phenomena

occurring during laser/material interaction are very close to the welding case.
Briefly, the electromagnetic wave (the laser) travel through a shielding gas and interacts with the metallic material. This interaction produces a high heat input leading to the local melting and vaporization of the material. During a vaporization process, metal atoms are ejected from the liquid-gas boundary. Due to the local momentum conservation, if particles are leaving the boundary, a "force" is produced in the opposite direction. The whole discussion here is about the way to simulate this mechanical effect. In most works, a pressure is applied on the liquid boundary, it's called the recoil pressure. This formulation is convenient due to its well-known physical bases as Clausius-Clapeyron saturation pressure [18]. It's also a very easy method to implement and to resolve. The only, missing point is the metal out going from the liquid to the gas phase. Indeed, theoretically, the vapor is ejected with a certain velocity. With the recoil pressure formulation, this part is totally neglected. The second formulation is based on the momentum conservation at the interface, so in the present paper we will call it, the "momentum" formulation. The principle, detailed in the following parts is quite simple, a mass is added in the gas phase, close to the evaporating boundary, and as we solve the momentum conservation, this mass produces implicitly a momentum. This technic is better physically speaking but is also known to disturb the numerical resolution.

Geometry

The simulated geometry is a cube composed by two main volumes, the gas on the upper part (z>0) and the metal on the bottom part (z<0) (Figure 1). These domains are only used to mesh setup. It should be noted that the physical domain and the powder does not appears yet because it is not considered as a geometrical entity but as an analytical initialization law in the Phase Field free boundary problem. This "handmade" initialization allows a computation with a homogeneous mesh and makes easier the first steps of resolution.

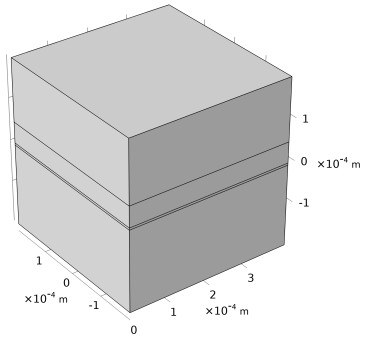

Figure 1 : Simulated geometry

The illustrated geometry on figure1 is a cube with 400 μm side length. This is set to simulate a simple elementary static laser case (no feeding rate) representative of a realist laser/material interaction time. It should be recalled that the size of the numerical problem is a real limitation for this kind of simulation and as we just want to check the validity of the formulation, a moving case is not yet necessary.

Governing Equations

As explain before, this case is multiphysics, coupling heat transfers and liquid/gas fluid flows; and multiphases; through the presence of solid, liquid, gas and powder.
Before introducing the mathematical formulation of physical phenomena and conservation principles, the free boundary tracking method has to be detailed.

Free boundary

Here the free boundary is supposed to be the whole interface between metal and gas, as well solid as liquid. The method used here is the Phase Field approach simulating a continuous boundary transportation thanks to the Cahn-Hilliard equation:

$$\frac{\partial \phi}{\partial t} + \vec{v}.\overrightarrow{\nabla \phi} = \vec{\nabla}.\gamma\overrightarrow{\nabla G} \qquad (1)$$

G is like a potential and γ is the mobility, determining the time scale of the diffusion phenomena. Both are purely numerical parameters in the present case. In the developed formulation, the previous equation can be written in the two following second order PDE solving respectively the Phase Field variable ϕ and the auxiliary variable ψ:

$$\frac{\partial \phi}{\partial t} + \vec{v}.\overrightarrow{\nabla \phi} = \vec{\nabla}.\frac{\gamma\lambda}{\varepsilon^2}\overrightarrow{\nabla \psi} \qquad (2)$$

$$\psi = -\vec{\nabla}.\varepsilon^2\overrightarrow{\nabla \phi} + (\phi^2 - 1)\phi + \frac{\varepsilon^2}{\lambda}\frac{\partial f}{\partial \phi} \qquad (3)$$

ε is the interface thickness parameter and λ is called the density of mixture energy and link the surface tension to the thickness parameter. $\partial f/\partial \phi$ is an additional energy input.
Due to a specific initialization, the Phase Field variable ϕ is constrained to take values between -1 and 1 with a continuous transition zone defined from ε through a hyperbolic tangent law (for more details, reader can refer to Comsol User Guide).

The boundary settings are for the sides, a "wetting" condition $\vec{n}.\frac{\gamma\lambda}{\varepsilon^2}\overrightarrow{\nabla \psi} = 0$ and $\vec{n}.\varepsilon^2\overrightarrow{\nabla \phi} = \varepsilon\left|\overrightarrow{\nabla \phi}\right|$. The upper boundary is set to an outflow condition.
The initial condition here is the initial shape of the interface (solid substrate and solid grains). As each particle radius and coordinates come from a previous DEM simulations (Figure 2 – [19]), authors have analytically built a function ϕ_{init} from this input data $p(x_0,y_0,z_0,r_0)$, particle centers and radii.

$$\phi_{init} = N_p - tanh\left(\frac{z-z_0}{\varepsilon\sqrt{2}}\right) - \sum_{i=0}^{N_p} tanh\left(\frac{\sqrt{(x-x_0^i)^2+(y-y_0^i)^2+(z-z_0^i)^2}}{\varepsilon\sqrt{2}} - {r_0}^i\right) \quad (4)$$

N_p is the total amount of particles, the second term is the flat interface located at $z_0 = 0\ mm$ and the third one is sum of N_p particles p_i located at (x^i_0, y^i_0, z^i_0).

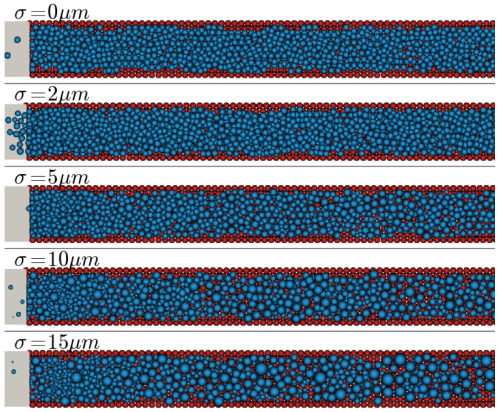

Figure 2: Illustration of results coming from DEM simulations ([19], blue is particles and red is the substrate).

The methodology to link DEM results to Comsol Multiphysics® models through Java Programming, has been presented in detail in [7]. Thus, authors will not recall this point in the present paper.

The figure 3 illustrates the "boundary" ($\phi = 0$) set as initial condition. The reader can see the powder grains appearing directly and without any geometrical entities.

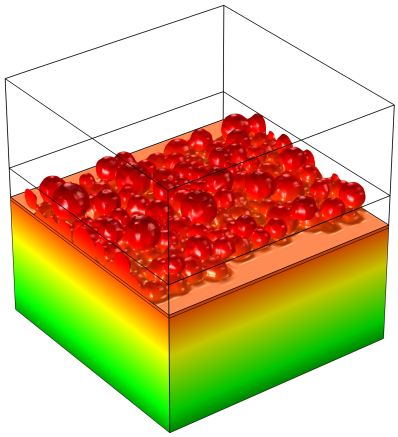

Figure 3: Initialization of the ϕ variable (the shown field is $\phi > 0$).

Heat transfers

As the material can be, now, identified (gas $\phi = -1$ and metal $\phi = 1$), the first conservation principle to consider is the heat conservation:

$$\rho_\emptyset {c_p}_\emptyset^{eq}\left[\frac{\partial T}{\partial t} + \vec{v}.\overrightarrow{\nabla T}\right] = \vec{\nabla}.\left(\lambda_\emptyset \overrightarrow{\nabla T}\right) + S\delta\emptyset \quad (5)$$

ρ, ${c_p}^{eq}$ and λ are respectively the density, the equivalent specific heat and the thermal conductivity. The ϕ indication describe the dependence to the phase, and S, detailed in *eq. 6* and *7* is the heat input/output such as the laser beam and evaporation latent heat. Due to the current Eulerian free boundary description (smoothed) of the metal/gas interface, these interfacial phenomena have to be introduced in the bulk through the $\delta\emptyset$ function, the Phase Field variable normal derivative.

$$S = \varphi_{laser}(t) - \dot{m}L_{vap} \quad (6)$$

$$\varphi_{laser}(t) = \frac{\alpha P_0}{\pi R_0^2} n_z[(x-x_0)^2 + (y-y_0)^2 < R_0^2] \quad (7)$$

n_z is the z component of the normal vector and α is the absorptivity. P_0, R_0 are respectively the laser power, the beam radius.

$\dot{m}L_{vap}$ is the vaporization enthalpy, calculated from the evaporated mass rate $\dot{m}$ and the latent heat L_{vap}. The first one comes from the Hertz-Langmuir and Clausius-Clapeyron [18] equations and the second one comes from the literature data.

$$\dot{m} = p_{sat}(T)\sqrt{\frac{M}{2\pi RT}}(1-\beta_r) \quad (8)$$

$$p_{sat} = p_0 exp^{\frac{ML_v}{R}\left(\frac{1}{T_v}-\frac{1}{T}\right)} \quad (9)$$

The side thermal boundary conditions have no real impact due to the formulation of the problem. As the heat source is assumed far from the boundaries, and as the dynamic is very fast, the domain boundary temperature does not change. A thermal insulation ($\varphi = 0$) is a good approximation.
Conversely, the upper face is submitted to the flow leaving the domain, thus the heat transport is allowed.
The radiative loss is neglected here assuming the evaporation flux much larger.

The initial condition is the ambient temperature, set here at *293 K*.

Fluid flows

As for the thermal problem, the fluid calculation is made in the whole geometry and phase properties are defined with a ϕ variable dependence.

$$\rho_\emptyset\left[\frac{\partial \vec{v}}{\partial t} + (\vec{v}.\vec{\nabla})\vec{v}\right] = \vec{\nabla}.\left(pI + \mu_\emptyset(\vec{\nabla}\vec{v} + (\vec{\nabla}\vec{v})^T\right) + (\sigma\kappa + \{p_{rec}|0\}).\delta\phi \quad (10)$$

$$\vec{\nabla}.\vec{v} = \left\{0\middle|\dot{m}\left(\frac{1}{\rho_v}-\frac{1}{\rho_l}\right)\delta\phi\right\} \quad (11)$$

Equations *10* and *11* are respectively, momentum and mass conservations. In these two equations, the terms $\{...|...\}$ is related to the two assumptions to treat the vaporization (detailed in the next part):

- The left-hand side $\{... \mid$ is the part corresponding to the recoil pressure formulation.
- The right-and side $\mid ... \}$ corresponds to the momentum conservation formulation.

ρ still the density and μ is the dynamic viscosity of each phase. As previously, the interfacial phenomena; the Laplace pressure $\sigma\kappa$ and usually the recoil pressure p_{rec} ([18], [20], [21] and [22]) are applied in the domain through the delta function $\delta\phi$.

The initial conditions in velocity and (relative) pressure are set to zero.
The boundary conditions are, no slip ($\vec{v} = \vec{0}$) for the metal boundaries and a reference pressure ($p = 0$) for the gas boundaries allowing a potential outflowing.
The flow in the solid metal is annealed thanks to an "penalized" viscosity appearing with a Heaviside function, for temperature lower than the solidus temperature $\mu(T) = \mu_0 + 10^6.H(T - T_s)$.

Vaporization details
It should be noted here that the process of vaporization leads to a deflection of the liquid upper boundary, creating the vapor capillary or keyhole. Numerically, two methodologies can produce this effect:

- Firstly, setting the recoil pressure at the liquid/vapor interface (p_{rec} *eq. 12*) but this method assumes a poor effect of the vapor shearing on the molten pool [23] (the realistic gas behavior is neglected).

It should be noted that for our Phase Field formulation, the recoil pressure can be introduced in the $\partial f/\partial\phi$ in *eq. 3* source term and in *eq. 10*.

$$p_{rec} = p_0 + p_{sat}\frac{(1+\beta_r)}{2} \qquad (12)$$

β_r is the retro-diffusion coefficient [20] set to a constant value here due to the high vaporization rate. Moreover, one must modify this formulation to simulate the gas accurately [24] (not done here).

- Secondly, writing the momentum conservation at the liquid/vapor interface leads to the modification of the mass conservation (*eq. 11, right side*) and Phase Field transport equation (*eq. 2*) as fallow [25]:

$$\frac{\partial\phi}{\partial t} + \vec{v}.\overrightarrow{\nabla\phi} - \dot{m}\left(\frac{V_{\phi 1}}{\rho_v}\right)\delta(\phi) = \vec{\nabla}.\frac{\gamma\lambda}{\varepsilon^2}\overrightarrow{\nabla\psi} \qquad (13)$$

With ρ_v the vapor metal density and $V_{\phi 1}$ the gas phase proportion in the transition layer.
The ρ_v can be approximated by three assumptions, a constant value, ideal gas law and corrected ideal gas law (considering the mesh size). In the present case, the vapor is assumed to be an ideal gas.

In order to validate the implementation of second technic in our numerical tool, both formulations have been tried and results are shown in the next section.

Numerical considerations

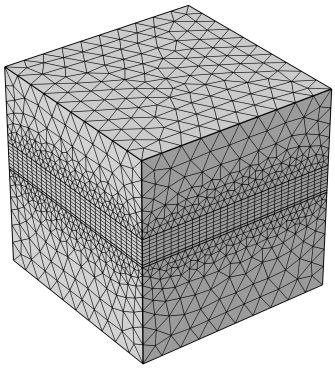

Figure 4: Illustration of the mesh.

As the particles have radii in the range [*4 µm*, *31 µm*], the mesh elements have to be close to the micrometer. Inside the powder zone the elements are quadrangular with *15 µm* maximum size and the remaining domains is meshed with freely growing tetrahedral elements.
This numerical settings, i.e. linear elements for heat, momentun and mass conservation equations and quadratic elements for the Phase Field problem, produces almost 300,000 DDL to solve.

The computation was done on Xeon Gold 6248R CPU with 10 active cores. It tooks slightly less than 9 hours to simulate 200µs (t_{pulse}: interaction time corresponding to LPBF process).

Material and process properties

In this case of methodology validation, the material does really matter, nevertheless, to be consistent, the numerical case was very close to current experimental investigation of LPBF on stainless steel (AISI 316L). The material properties were assumed to be constants for a given phase (metal and gas) and are summarized in the tables 1, 2, 3 and 4.

***Table 1**: Process parameters (Yb-YAG laser)*

Process properties	Symbol	Value
Laser Power (W)	P_0	720
Beam radius (µm)	R_0	100
Interaction time (µs)	t_{pulse}	200

Results and discussions

As explained previously, two methodologies of vaporization process or effect can be found in the literature. The present work is made to check the validity of our formulation (*eq. 10* and *eq. 11*). The simulated case is a static laser configuration with

720W power during 200µs. In both cases, the beam still the same, i.e. a 100µm radius tophat beam.

***Table 2**: Metal properties (AISI 316L)*

Material properties	Symbol	Value
Thermal conductivity (W/m/K)	λ	35
Density (kg/m^3)	ρ	7200
Specific heat (J/kg/K)	c_p	760
Melting point (K)	T_m	1712
Solidus (K)	T_s	1697
Liquidus (K)	Tl	1727
Melting range (K)	DT	30
Boiling point (K)	T_v	3100
Latent heat fusion (J/kg)	L_m	2.47 10^5
Latent heat vaporization (J/kg)	L_v	5.52 10^6
Molecular mass (g/mol)	M	55.8
Retrodiffusion coef.	β_r	0.17
Dynamic viscosity (Pa.s)	μ_0	0.006

***Table 3**: Shielding gas properties (Air)*

Material properties	Symbol	Value
Thermal conductivity (W/m/K)	λ	0.012
Density (kg/m^3)	ρ	1.2
Specific heat (J/kg/K)	c_p	1000
Molecular mass (g/mol)	M	28.8
Dynamic viscosity (Pa.s)	μ	1 10^{-5}

***Table 4**: Numerical properties*

Material properties	Symbol	Value
Interface thickness (µm)	ε	2.5
Mobility parameter	χ	$f(\vec{v})$

In both cases, shown in the Figure 5, the physical and numerical settings are perfectly similar. The vapor mechanical effect is just set as a pressure in the upper case and as a momentum interface transfer, in the lower case.

Two observations have to be highlighted. Firstly, the molten and vaporized areas are very similar. Secondly, the liquid behaviors are not perfectly the same. As the gas flow is not neglected in the last case, one can observe liquid ejections resulting from the gas shearing upon the liquid. This mechanism, usually neglected, is responsible of the slight differences between the two simulations.

Looking more precisely at the drilling dynamics (Figure 6), two points can be spotlighted. Firstly, the vaporization process starts at the same moment and the firsts molten pool shapes are very close (*120-140 µs*). This is mainly due to the equivalence of the thermal problems before and during the first steps of vaporization process. Secondly, after few tens of microseconds (160-200 µs), the maximum boundary

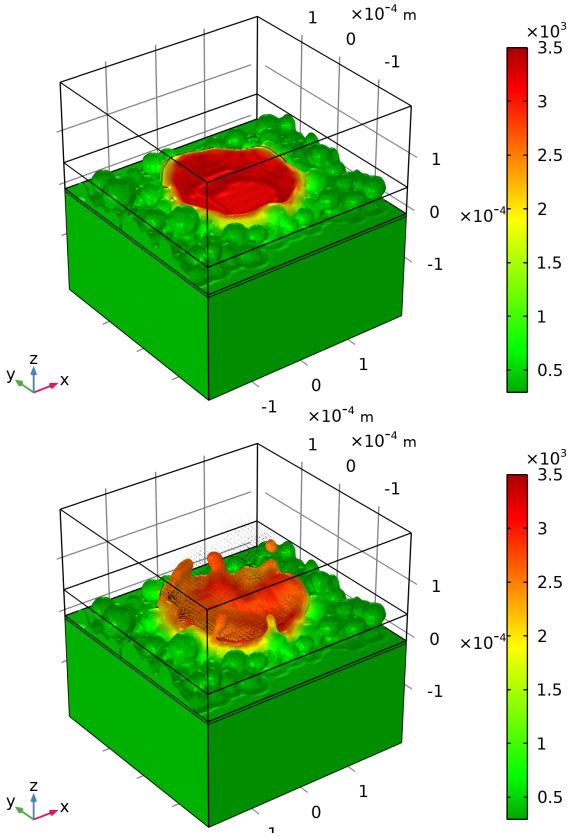

Figure 5: 3D comparison between pressure (upper part) and momentum (lower part) formulations - Color bar is the temperature (K).

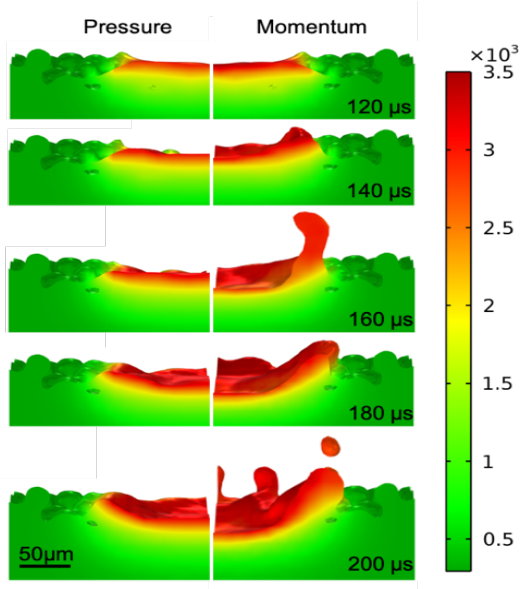

Figure 6: Capillary cross section (left part: pressure formulation - right part: momentum formulation); color bar is the temperature (K).

deflection is higher with the momentum formulation than with the pressure. This is a particular effect of the shearing. As the time increase, the "capillary''

(the hole) thickness increases and stronger is the interaction between gas and liquid. This is quite clear looking at the 160µs and 200µs cases, the vapor drags the liquid at the periphery of the molten pool (drops and ejections) reducing the liquid thickness and thus, increasing the penetration. This phenomenon is amplified with the interaction time and is confirmed by the maximal temperature values shown in the Figure 7.

Indeed, as assumed previously, the velocities of the gas (dashed lines) and the liquid (lines) are much higher in case of the momentum formulation (in blue). The high lateral motion of the liquid (momentum case) can be correlated to the lower temperature observed during vaporization. Indeed, as the hottest part of the molten pool is below center of the laser beam, the radial motion of the fluid transports the heat from the center to the side, i.e., from the hottest to the coldest part of the liquid surface creating a kind of homogenization. It should be noted that, although no detailed experimental validation has been done for this first test case, the vapor maximal velocities are much more realistic for this process range (around 200m/s) [26] than the values seen in the literature [23, 25].

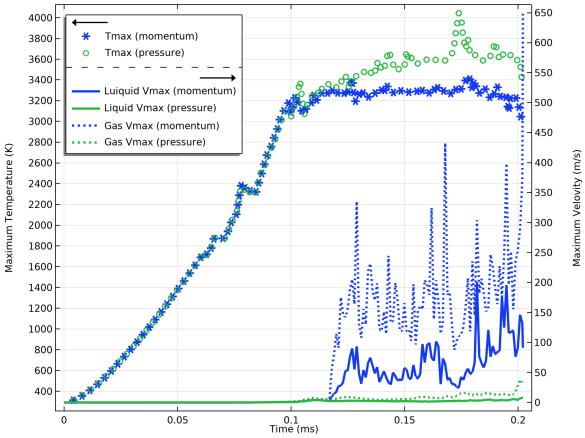

Figure 7: Maximum temperatures and velocities for pressure and momentum formulations (dots: temperatures - lines: liquid velocities - dash lines: gas velocities)

Conclusions and perspectives

In this paper, authors have illustrated the way to simulate the indirect effect of the vaporization process on the melt pool dynamics. Indeed, after a brief description of the model (physically and numerically), a comparison between a "pressure" formulation and a "momentum" formulation have been done. An ejection phenomenon is then highlighted and seems to be directly related to the vapor jet (or plume) consideration. At the end, the maximum gas velocities are plotted in both cases, and, regarding the literature, the momentum formulation seems to be more predictive than pressure. The strong effect of the gas flow on thermal field, was also demonstrated. Thus, the common assumption of the recoil pressure applied on the gas/liquid boundary for laser applications, seems to be too strong to allow simulation of process stability. To illustrate the perspectives of this kind of simulation (momentum formulation), several "moving" cases have been done for different linear energy (1333J/m and 969J/m) and results illustrate less ejections for the lower energetic case.

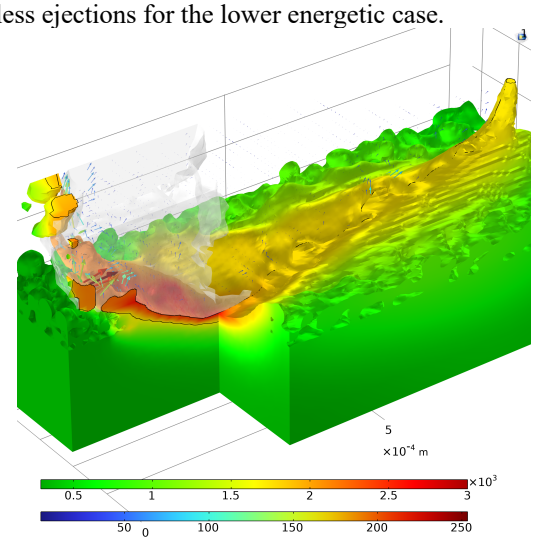

Figure 8: LPBF simulation case 1 - 720W 0.55m/s (El = 1333J/m) Colorfield is temperature, color vector are velocity amplitude.

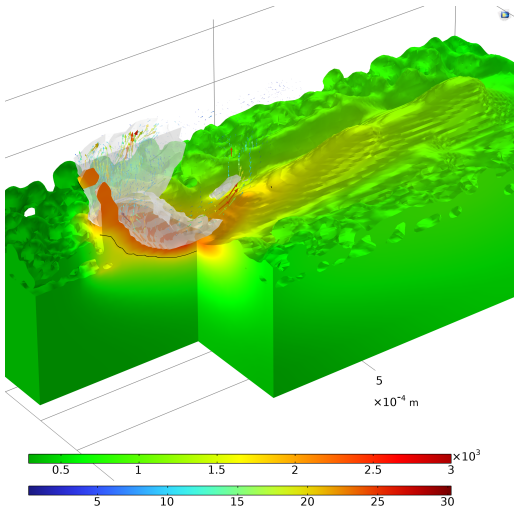

Figure 9:LPBF simulation case 1 - 320W 0.33m/s (El = 969J/m) Colorfield is temperature, color vector are velocity amplitude.

References

[1] T. DebRoy, H.L. Wei, J.S. Zuback, T. Mukherjee, J.W. Elmer, J.O. Milewski, A.M. Beese, A. Wilson-Heid, A.Ded, W. Zhang, "Additive manufacturing of metallic components – Process, structure and properties", *Progress in Materials Science 92,* pp. 112–224, 2018.

[2] V. Gunenthiram, P. Peyre∗, M. Schneider, M. Dal, F. Coste, I. Koutiri, R. Fabbro, "Experimental analysis of spatter generation and melt-pool behavior during the powder bed laser beam melting process", *Journal of Materials Processing Tech. 251*, pp. 376–386, 2018.

[3] V. Gunenthiram, P. Peyre, M. Schneider, M. Dal, F. Coste, I. Koutiri, R. Fabbro, "Experimental analysis of spatter generation and melt-pool behavior during the powder bed laser beam melting process", *Journal of Materials Processing Technology - Vol. 251*, pp. 376-386, 2018.

[4] I. Yadroitsev∗, A. Gusarov, I. Yadroitsava, I. Smurov, "Single track formation in selective laser melting of metal powders", *Journal of Materials Processing Technology 210*, pp. 1624–1631, 2010.

[5] D.L. Bourell, "Perspectives on additive manufacturing", *Annual Review of Materials Research 46*, 2016.

[6] Wohlers, T. T., & Caffrey, T., "Wohlers report 2013: additive manufacturing and 3D printing state of the industry", *Annual worldwide progress report*, 2013.

[7] M. Dal, Y. Mayi, K. Marchais, P. Peyre, "Powder Consideration for Additive Manufacturing Simulation", *Comsol Conference*, 2020.

[8] S. Kolossov, "3D FE simulation for temperature evolution in the selective laser sintering process", *International Journal of Machine Tools & Manufacture* 44, pp. 117–123, 2004.

[9] M. Dal, "A new equivalent approach for additive manufacturing (SLM) numerical simulation", *35th International Congress on Applications of Lasers and Electro-Optics*, San Diego (USA), 2016.

[10] Q. Chen, "Three-dimensional finite element thermo-mechanical modeling of additive manufacturing by selective laser melting for ceramics materials", *Additive Manufacturing* 16, pp. 124-137, 2017.

[11], P Zehner, "Wärmeleitfähigkeit von Schüttungen bei mäßigen Temperaturen », *EU Schlünder - Chemie Ingenieur Technik, Wiley Online Library,* 1970.

[12] M. Rombouts, "Photopyroelectric Measurement of Thermal Conductivity of Metallic Powders", *Journal of Applied Physics 97,* 024905, 2005.

[13] Saad A. Khairallah, Andrew T. Anderson, Alexander Rubenchik, Wayne E. King, "Laser powder-bed fusion additive manufacturing: Physics of complex melt flow and formation mechanisms of pores, spatter, and denudation zones", *Acta Materialia 108*, pp. 36-45, 2016.

[14] Mohamad Bayat, Sankhya Mohanty, Jesper Henri Hattel," Multiphysics modelling of lack-of-fusion voids formation and evolution in IN718 made by multi-track/multi-layer L-PBF", *International Journal of Heat and Mass Transfer 139*, pp. 95–114, 2019.

[15] L. Cao, "Mesoscopic-scale simulation of pore evolution during laser powder bed fusion process", *Computational Materials Science 179*, 109686, 2020.

[16] Mayi, Y. A., Dal, M., Peyre, P., Bellet, M., Metton, C., Moriconi, C., & Fabbro, R.,"Transient dynamics and stability of keyhole at threshold in laser powder bed fusion regime investigated by finite element modeling", *Journal of Laser Applications 33*, 2021.

[17] Daligault, J., Dal, M., Gorny, C., Coste, F., & Fabbro, R., "Combination of Eulerian and ray-tracing approaches for copper laser welding simulation", *Journal of Laser Applications 34(4)*, 2022.

[18] A.A. Samokhin, "Effect of Laser Radiation on Absorbing", Condensed Matter, Nova Science Publishers, 1990.

[19] K. Marchais, J. Girardot, C. Metton, I. Iordanoff, "A 3D DEM simulation to study the influence of material and process parameters on spreading of metallic powder in additive manufacturing", *Computational Particle Mechanics*, 2021.

[20] K. Hirano, "Experimental determination of temperature threshold for melt surface deformation during laser

interaction on iron at atmospheric pressure", *Journal of Physics D, Applied Physics 44*, 435402, 2011.

[21] C.J. Knight, "Theoretical modeling of rapid surface vaporization with back pressure", *AIAA Journal 17*, 5p, 1979.

[22] A. Matsunawa, "The simulation of front keyhole wall dynamics during laser welding", *Journal of Physics D: Applied Physics* 30, pp. 798-809, 1997.

[23] A. Queva, G. Guillemot, C. Moriconi, C. Metton, M. Bellet, "Numerical study of the impact of vaporisation on melt pool dynamics in Laser Powder Bed Fusion - Application to IN718 and Ti–6Al–4V", *Additive Manufacturing 35*, 101249, 2020.

[24] S. Pang, X. Chen, J. Zhou, X. Shao, C.Wang, "3D transient multiphase model for keyhole, vapor plume ,and weld pool dynamics in laser welding including the ambient pressure effect", *Optics and Lasers in Engineering 74* pp. 47–58, 2015.

[25] M. Courtois, M. Carin, P. Le Masson, S. Gaied, M. Balabane, « A complete model of keyhole and melt pool dynamics to analyze instabilities and collapse during laser welding", *Journal of Laser Applications 26 (4)*, pp. 042001, 2014.

[26] Mayi, Y. A., Dal, M., Peyre, P., Bellet, M., Metton, C., Moriconi, C., Fabbro, R., "Laser-induced plume investigated by finite element modelling and scaling of particle entrainment in laser powder bed fusion*", Journal of Physics D: Applied Physics 53(7)*, 075306, 201